Geochemical Modeling of Engineered Water Injection in Carbonates under Harsh Conditions: New Insights with Ionic Adsorption

DOI:
10.1115/1.4054956

Journal of Energy Resources Technology, 145 (2), 023004

Geochemical Modeling of Engineered Water Injection in Carbonates under Harsh Conditions: New Insights with Ionic Adsorption

Ilyas Khurshid*
Department of Mechanical Engineering, Khalifa University, Abu Dhabi, P.O.Box 12277, UAE.
ilyas.khurshid@ku.ac.ae

Emad W. Al-Shalabi,
Department of Petroleum Engineering, Khalifa University, Abu Dhabi, P.O.Box 12277, UAE.
emad.walshalabi@ku.ac.ae

Imran Afgan,
Department of Mechanical Engineering, Khalifa University, Abu Dhabi, P.O.Box 12277, UAE.
Imran.afgan@ku.ac.ae

Bilal Khurshid,
Department of Industrial Engineering, University of Engineering and Technology Peshawar, Pakistan.
bilal.khurshid@uetpeshawar.edu.pk

Anas M. Hasan,
Department of Petroleum Engineering, Khalifa University, Abu Dhabi, P.O.Box 12277, UAE.
anas.hasan@ku.ac.ae

Abstract

Carbonates are characterized by low oil recovery due to their positive surface charge and consequent high affinity to negatively charged crude oil, rendering them to a state of mixed-to-oil wettability. In order to understand the rock/brine/oil interactions and their effect on potential-determining-ions (PDIs) adsorption/desorption during engineered water injection is needed for realistic and representative estimations of oil recovery. Therefore, this study reveals a novel approach to capture various interactions and better predict the effect of PDIs adsorption/desorption as well as concentrations of various ionic species in the effluent using Phreeqc. In this work, we determined adsorption/desorption of PDIs for the first time using surface complexation reactions and then we validated our results with experimental data from the literature. Our results showed that the presence of PDIs and their respective adsorption/desorption results in surface charge decrease and increase in pH. Also, this study found that ionic adsorption depends on ionic strength and species activity where calcium adsorption remained constant while magnesium and sulfate adsorptions varied with ionic strength. Moreover, magnesium ion was found to be the most sensitive ionic species to temperature as opposed to calcium and sulfate ions. In addition, sulfate spiking and dilution decrease the sulfate adsorption since the sulfate starts reacting with magnesium and forming complexes. Additionally, deionized water resulted in the highest charge decrease and pH increase with related incremental oil recovery. The adsorption/desorption of ions is case-dependent and thus, the findings cannot be generalized.

Keywords: Surface Complexation; Potential Determining Ions; Adsorption/Desorption; Carbonates; Low Salinity/Engineered water Injection

* Corresponding Author.

1. Introduction and Background

Carbonate reservoirs hold a significant portion of the global hydrocarbon (oil and gas), which is estimated about 50-60% of crude oil and 40-50% of gas reserves. Nevertheless, the recovery factor (RF) from carbonates is lower than 35% [1]. This low RF from carbonate reservoirs is due to reservoir heterogeneity, complex structures, low permeability, and mixed-to-oil wet condition [2]. Thus, during conventional recovery (primary and secondary) from carbonates, the yield is less than 35% of the original oil in place [3-4]. This leaves a significant volume of oil remains trapped and unswept in these reservoirs. Therefore, the implementation of enhanced oil recovery (EOR) techniques can boost oil recovery for carbonate reservoirs. In the last couple of decades, ample research has been conducted in the field of changing carbonate wettability toward a hydrophilic (water-wetting) state and hence, improving the recovery of oil. This is because the RF is dependent on formation wettability and if the oil-wet conditions prevail, the recovery of oil remains at the lowest level [5-6]. Usually, carbonates are found to be intermediate to fully oil-wet, which is related to their positively charged surface and the adsorbed negatively charged acidic groups present in the crude oil.

Low salinity/engineered water injection (LSWI/EWI) is one of the potential techniques that has been proved to enhance oil recovery by several researchers through their laboratory and numerical works [7-19]. LSWI refers mostly to water dilution while EWI refers to ion-modification of injected water including hardening and softening of particular ions [2]. The results showed that the modification of wettability is the foremost factor behind additional oil recovery, particularly in carbonates [13]. Moreover, the process of wettability alteration is a complex phenomenon and it is controlled by several mechanisms such as the release and transport of clay particles [7], dissolution of calcite [12], dissolution of anhydrite [14], rock surface charge modification [9-10], pH increase [2], electro-kinetics at rock-brine-oil interfaces [17], micro-dispersion formation [16] and stability of the wetting film [18]. It is observed that during EWI, one of these mechanisms or their combination disturbs the reservoir equilibrium and causes the substitution/adsorption of some potential determining ions (PDIs) including Ca^{2+}, Mg^{2+}, and SO_4^{2-}, and hence, wettability alteration occurs.

It is worth mentioning that in laboratory-based static and dynamic experiments, pure minerals are used to determine the adsorption of PDIs (Ca^{2+}, Mg^{2+}, and SO_4^{2-}), and the adsorption behavior of these PDIs on carbonates surfaces is seldom the same due to the heterogeneity in carbonate mineralogy and reservoir conditions. This effect becomes more significant in the presence of trace minerals such as anhydrite, clay, ankerite, magnesite, and metal oxides [20-21]. Moreover, carbonate surface charges and dissolution behaviors differ based on the respective carbonate mineralogy. The point of zero charges for metal oxides present in carbonates is usually higher than calcite [22]. Thus, at certain pH, the metal oxides and carbonate surfaces would have an opposite sign [23]. Consequently, the overall surface potential will vary spatially in carbonates [24] and the determined zeta potential of carbonate can't be the perfect mechanism to describe charge-dependent adsorption and dynamics [25].

Furthermore, when the injected low salinity water contacts the rock surface, its composition would differ from the injected one due to formation dissolution. Generally, the adsorption of divalent anions decreases with the reservoir pH [26] and increases slightly with ionic strength and divalent ions concentration. Moreover, Southwick *et al.* [27] mentioned that with the change in water chemistry, the adsorption of different ions on metal oxide sites over the edges of platelets-clay present in carbonates can change unevenly in magnitude and dynamics. In fact, after performing experiments on oxidized rock outcrops containing a substantial amount of montmorillonite clay and iron, Levitt and Bourrel [28] observed that the adsorption could be reduced by rinsing the surface with sodium chloride. They also observed that the exchange of divalent cations results in lowering the surface charge and the related adsorption.

Therefore, the adsorption dynamics of Ca^{2+}, Mg^{2+}, and SO_4^{2-} during EWI needs further investigation at various salinities. Additionally, the adsorption of PDIs depends on rock surface chemistry, water composition,

chemical characteristics, and different functional groups found in the reservoir. However, for carbonate rocks because of heterogeneity in their mineralogy and surface chemistry, the prediction of the extent and dynamics of potential determining ions adsorption is even more challenging. Considering these aspects, this work aims at interpreting different processes that control ion adsorption such as the structure of the adsorbed layer (monodentate or multidentate), mechanisms of adsorption, and kinetics adsorption for different ions that control the oil recovery during LSWI/EWI. The objective of this research is to determine the adsorption dynamics of different potential determining ions during EWI. We developed a geochemical-based numerical model to explore the interactions between carbonate surface and injected engineered water. The coreflooding data performed by Shehata *et al.* [29] was used for validation where they used Indiana limestone in their coreflooding experiments. We performed several simulation runs for their experiments to determine the adsorption behavior of PDIs for the first time, to investigate the effect of different injected water compositions. We characterized the various properties of Indiana limestone, its bulk, and surface mineralogical compositions along with the initial and evolved composition of injected water. We used surface complexation modeling in PHREEQC [30] to estimate the carbonate dissolution kinetics to trace the change in injected water composition. The surface complexation calculations were performed by implementing the diffuse layer model. This approach helped in predicting the surface speciation with the change in reservoir fluid compositions. In Indiana limestone, the two major surfaces are calcite and trace minerals such as oxide sites on the edges of minerals that differ in their magnitude of surface charge, point of zero charges values, surface chemistry, and specific area. Thus, based on our novel investigation a set of surface complexation reactions are defined for the adsorption of PDIs on mineral surfaces/surface groups through monodentate and weak complexation. Besides, the effect of four influential parameters on PDIs adsorption is investigated including ionic strength, reservoir temperature, sulfate spiking, and sulfate dilution. This study provides new insights into understanding the adsorption of different PDIs in carbonates and their related effect on oil recovery during EWI. The adsorption/desorption of ions is case-dependent and thus, the findings cannot be generalized.

2. Model Description and Development

2.1 Adsorption/ desorption Geochemical/Numerical Model

The presence of crude oil and connate water in carbonates is controlled by rock wettability and the latter is affected by many factors. The important factors such as crude oil composition and salinity of injected water on reservoir wettability have been mainly investigated [31-32]. The experimental outcome of their results showed that the carbonate wettability changes with the variation in the salinity of the injected water. During the injection of LSW, the ionically tuned water changes the force distribution at the micro-level at the rock surface interface where the adsorption of ions to the rock surface depends on the surface potential. This potential at the surface is controlled by the surface charge, and the latter is defined by the adsorbed species. Therefore, adsorption of ionic species modifies the oil-water characteristics at the interface and alters the rock to a more water-wetting state as shown in **Fig. 1**. Thus, the trapped oil would release from the reservoir surface in a free flow fluid state, as soon as the negatively charged divalent ion adsorbs on the positively charged carbonate surface. This phenomenon is characterized by the disjoining pressure to capture the related effect on oil recovery. This disjoining pressure is represented by Π_t and it depicts the magnitude of water film stability [33-34], which should satisfy the following equation:

$$\Pi_t(h) = \Pi_s(h) + \Pi_{Vdw}(h) + \Pi_{EDL}(h) \quad , \tag{1}$$

where Π_s is the repulsive structure force, $\Pi_{EDL}$is the double-layer repulsive force, and Π_{Vdw} is the van der Waals forces. The detailed equations are as follows:

$$\Pi_s(h) = A_s exp\left(-\frac{h}{h_o}\right), \tag{2}$$

$$\Pi_{EDL}(h) = n_b kT \frac{(2\psi_{r1}\psi_{r2}\cosh(\kappa h) - \psi_{r1}^2 - \psi_{r2}^2)}{(\sinh(\kappa h))^2} \quad , \tag{3}$$

$$\Pi_{VdW}(h) = -\frac{A\left(15.96\frac{h}{\lambda}+2\right)}{12\pi h^3\left(1+5.32\frac{h}{\lambda}\right)^2} \quad , \tag{4}$$

where h is the distance of separation between the two surfaces (oil-brine and rock-brine), h_o is the length of decay

(0.05 nm), λ is the length (attenuation), n_b is the ion density, k is Boltzmann's constant and its value is 1.38×10^{-23} J/K, T is the temperature (Kelvin), A_s is a coefficient (1.5×10^7 kPa), ψ_{r1} and ψ_{r2} are the reduced potentials, A is the Hamaker constant, and κ is reciprocal length (Deby-Huckel).

The bulk mineralogical composition of carbonate reservoir rock is used to model rock dissolution kinetics and thus, the general expression for the specific dissolution rate is given by [30]:

$$r = r_{k1}a_{H+}^{n1}e^{\frac{-Ea1}{RT}} + r_{k2}a_{H_2O}^{n2}e^{\frac{-Ea2}{RT}} + r_{k3}a_{CO_2}^{n3}e^{\frac{-Ea3}{RT}} + r_{k1}a_{OH-}^{n4}e^{\frac{-Ea4}{RT}}, \quad (5)$$

where r is the specific dissolution rate (mol/m^{2}s), r_k is the rate constant, T is the temperature (K), R is the gas constant (8.3145×10^{-3} kJ/kmol), a_{H+} is the activity of the proton (dimensionless), E_a is the activation energy, and a and n are the activity and reaction order, respectively for hydrogen (H^+), water, carbon dioxide (CO_2), or hydroxide (OH^-). The dissolution rate for minerals (except calcite) was calculated by [35]:

$$\frac{dm}{dt} = rim_0\frac{S_A}{V}\left(\frac{m}{im_0}\right)^n(1-\Omega), \quad (6)$$

where S_A is the surface area (m^2/mol), im_0 is the initial moles of mineral per unit volume (1 L, or kg water- kgw), m is the current moles of mineral per solution volume $(m/im_0)^n$, n with a value of 0.67 is a correction factor to account for changes in S_A/V during the dissolution of the mineral, and Ω is the saturation state defined as the ratio of the ion-activity product to the solubility product (k_{sp}) for the solid. The initial mole of mineral (im_0) for a coreflood was calculated by [36]:

$$im_0 = \frac{\rho V(1-\phi)\omega}{\phi MW}, \quad (7)$$

where ω is the mass fraction of the mineral in bulk mineralogy, ϕ is porosity (0.215), ρ is the rock bulk density (2.2 g/cm^3), MW is the mineral molecular weight, and V is the solution volume (equivalent to PV) that is in 1 L.

2.1.1 Adsorption Analysis. To understand the mechanism behind EWI in carbonates, it is important to consider the aqueous species adsorption on the rock surface. Due to the large surface area of carbonates, they have high reactive surfaces, and consequently, they can adsorb a certain amount of ions. Therefore, in this study, we considered various models for ion adsorption during low salinity/engineered water injection.

2.1.2 Adsorption Measurement. The adsorption of various ionic species on the carbonate surface can be calculated by material balance through determining the change between the ionic concentration of the aqueous species in the injected water before and after adsorption. The adsorption of ionic species can be calculated using the following equation:

$$q = \frac{v(C_o-C_e)}{m}, \quad (8)$$

where q is the adsorption density of an ionic specie (mg/g), C_o is the primary concentration of ionic species (ppm), C_e is the equilibrium concentration of ionic species (ppm), m is the mass of the rock sample (g), and v is the solution volume (mL). The static adsorption can be calculated by matching the primary concentration of ionic species with their concentration after reaching/attaining equilibrium.

2.1.3 Adsorption Isotherms. These various models of adsorption isotherm are used to estimate the equilibrium between the concentrations of adsorbate that gather on the adsorbent and the magnitude of the dissolved adsorbate [37]. The different adsorption models used to determine the adsorption equilibrium behavior of a species are described below:

Freundlich Isotherm. This isotherm is the most convenient form of the isothermal equation, which is used to estimate the heterogeneous adsorption configuration with an insignificant saturation ratio of adsorbent to adsorbate. Therefore, this type of isotherm can predict infinite surface coverage and it shows multilayer adsorption on the solid surface. The number of ions adsorbed (q_e) can be calculated from this isotherm by the following equation:

$$q_e = K_f C_e^{1/n}, \quad (9)$$

where K_f is the ionic species adsorption capacity, and subscript *1/n* is the intensity of ion adsorption. The adsorption magnitude can be estimated from the adsorption intensity index (*1/n*). When *1/n* lies between 0.1 and 0.5, around this range the adsorption is considered to be promising. On the other hand, when *1/n* is between 0.5 and 1 the adsorption is easy to adsorb. However, it is challenging to adsorb when *1/n* is above the value of 1 [38]. The main disadvantage of the Freundlich isotherm is that it works at low solute concentration, but with the increase in the concentration of solute, it shows deviation.

Langmuir Isotherm. This type of isotherm is the most commonly used model to describe the process of ionic adsorption for a monodentate system. The following equation can be used to determine the maximum adsorption ability of an ionic species with this type of isotherm [39]:

$$q_e = \frac{q_o K_{ad} C_e}{1 + K_{ad} C_e}, \tag{10}$$

where q_e, q_o, C_e, and K_{ad} stand for the concentration of adsorbate per unit mass of adsorbent, amount to be adsorbed, the concentration of the adsorbate at equilibrium, and adsorption energy, respectively. The value of q_o is calculated from the slope and K_{ad} is estimated from the intercept of the straight line. However, the Langmuir isotherm assumes that the surface coverage is monolayer and the adsorption sites are homogenous and identical with equivalent energy. Another non-dimensional equilibrium parameter of Langmuir isotherm (L_{iso}) can be introduced to Eq. 10 to estimate the adsorption process and it is given as:

$$L_{iso} = \frac{1}{1 + K_{ad} C_e} \ . \tag{11}$$

The L_{iso} value shows that the process of adsorption is favorable when ($L_{iso} < 1$), unfavorable ($L_{iso} > 1$), linear ($L_{iso} = 1$), and for irreversible ($L_{iso} = 0$).

2.2 Model Development: Surface Complexation-based Ionic Adsorption Model

The surface complexation describes the sorption of ionic species based on the equilibrium of surface reactions. The surface complexation reactions are considered fast reactions and they are defined by reaction thermodynamics [30]. Thus, they present the adsorption of ions on the rock surface and thus form an electrical double layer (EDL). It is important to mention that EDL changes with the variation in the injected water composition. Therefore, depending upon the composition of EWI, a distinctive electrical potential would develop at the rock-brine-oil interface. It is imperative to mention that the EDL presents the distribution of various ionic species that surrounds the charged surface. The theory of EDL is based on the existence of two parallel layers known as the stern layer and the diffuse layer. These ionic layers originate around a rock surface. Moreover, the use of surface complexation models has several benefits in modeling the geochemistry behavior of a system over different adsorption models as discussed above. The adsorption models are quite simple and ignore the change in fluid composition, rock surface charge, solution ionic strength, and pH. Thus, surface complexation modeling used in this study is a more comprehensive approach and it can overcome the limitations posed by various adsorption models.

The potential at the mineral surface, stern layer, and slipping plane are known as surface potential, stern potential, and zeta potential, respectively. The first layer around the positively charged carbonate is the stern layer and it is composed of negative charged fixed ions adsorbed on the carbonate surface. At the boundary of this layer, a major drop of potential occurs and its thickness is usually 1 nm. The second layer is known as the diffuse layer and its thickness lies in the range between 1-500 nm subject to the rock surface charge and solution ionic strength. The ionic species in this layer are loosely attached to the rock surface via Coulomb force and can move in the solution controlled by electrical attraction. The ions opposite in charge to the surface charge of the mineral are attracted and similar charges are repelled. This process leads to the screening of the surface charge and thus, this layer splits into two regions. The first region is between the stern plane and the slipping plane. In this region, the ions are not affected by the fluid flow. The second region of the diffuse layer lies between the slipping plane and bulk fluid, ions in this region are controlled by the fluid flow. Thus, the flow of fluid disturbs the distribution of ions in this region.

In this study, we performed surface complexation and ion adsorption for the experimental investigation performed by Shehata *et al.* [29]. The XRD data for Indiana limestone cores used by the latter authors consist of 99% calcite. It was mentioned by Brady and Thyne, [40] that the calcite surface is composed of two sites: hydrated calcium sites (>CaOH) and carbonate sites (>CO_3H). The surface complexation reactions considered in this study are given in **Table 1-2** for the rock-brine interface. The surface of carbonate would attain a surface charge due to the existence of these sites. Thus, the calcite would gain or lose the hydrogen ions by adsorbing the corresponding anions or cations subject to the properties of charge on these sites. Moreover, **Table 3** shows the surface complexation reactions and their respective equilibrium constants for the oil-brine interface. It is important to mention that each of these surface complexation reactions has an equivalent mass-action equation. For example for CB-6, the inclusion of the electrostatic term in the equation below is described by the necessity of ionic species activities on the surface potential. Thus, the combined mass action equation is given by:

$$K_s = \frac{[>CaSO_4^-]}{[>CaOH_2^+][SO_4^{2-}]\exp(2F\psi_e/RT)} \quad , \tag{12}$$

where ψ_s, F, R, and T stand for surface potential, Faraday constant, universal gas constant, and temperature, respectively. If the carbonate surface potential is positive, then the negatively charged divalent species such as sulfate ion activity will increase close to the surface and it will decrease away from the surface. This phenomenon will lead to the removal of oil from the surface, adsorption of sulfate on the carbonate surface, and formation of complexes between positively charged divalent ions, such as Mg^{+2}, and Ca^{+2}, with crude oil. Therefore, the activities could be expressed in terms of surface concentrations.

It is important to mention that we used the Grahame equation to describe the correlation between surface potential and surface charge. The surface charge (σ_s) is determined in coulombs whereas the surface potential (ψ) is calculated in volts. Moreover, the Gouy Chapman model is used to derive the Grahame equation by Israelachvili, [41] and it is given as:

$$\sigma_s^2 = 8000\varepsilon\varepsilon_0 RTI\left[sinh\left(\frac{\nu F\psi}{2RT}\right)\right]^2, \tag{13}$$

where ε, ε_0, T, R, I, and ν stands for the dielectric constant, vacuum permittivity constant, temperature, universal gas constant, solution ionic strength, symmetric electrolyte ionic charge , respectively.

The temperature of a reservoir usually increases with the depth because of a continuous increase in the geothermal gradient. Therefore, for a typical carbonate reservoir, its temperature would be greater than 298.15 K. Thus, to model the aqueous reactions and dissolution/precipitation reactions in high-temperature reservoirs. It requires a systematic temperature correction for the various equilibrium constants. Where the temperature dependency is determined by utilizing the van't Hoff equation that is given as:

$$\frac{d[lnK_i(T)]}{dT} = \frac{\Delta H_i^o(T)}{RT^2}, \tag{14}$$

where ΔH_i^o is a function of temperature and for reaction (i), it is the standard heat of reaction. Thus, Equation (14) is integrated to get the generalized form of van't Hoff equation:

$$ln\frac{K_i(T_2)}{K_i(T_1)} = \frac{\Delta H_i^o}{R}\left(\frac{1}{T_1} - \frac{1}{T_2}\right). \tag{15}$$

For the various geochemical reactions (aqueous and dissolution/precipitation). Equation (15) is utilized to determine the respective equilibrium constant at temperature T_2 [42]. However, due to limited data available in the literature regarding the change in enthalpy for the various surface complexation chemical reactions. This study employed the following analytical equation to incorporate the dependence of temperature on surface complexation reactions to calculate their respective intrinsic stability constants as proposed by [42]:

$$Log_{10}K = A_1 + A_2T + \frac{A_3}{T} + A_4Log_{10}T + \frac{A_5}{T^2} + A_6T^2\,, \tag{16}$$

where the reservoir temperature (T) and different parameters A_1 - A_6 were attuned at 25 °C. **Tables 1**, **2**, and **3** show the temperature corrected respective intrinsic stability constant for various surface complexation reactions for calcite, dolomite, and oil at 90°C, respectively.

The advantages of using surface complexation for adsorption modeling include electrostatic interaction between aqueous species and charged surface, change in ionic strength and related variation in surface potential and surface charge, and variation of pH due to surface complexation reactions. Thus, the surface complexation is considered a comprehensive modeling technique as it captures the variation of surface charge, mineral sorption properties, and mineral site chemical structure. However, surface complexation modeling has uncertainties due to experimental data limitations. Moreover, the equilibrium constant and site densities may vary over a certain range. As discussed, the modification of formation wettability depends on the stability of water films, and this film stability is controlled by the structure of EDL. Thus, the application of the surface complexation model can effectively provide the change in rock wettability properties during low salinity water flooding. In surface-complexation reactions, the number of available adsorption sites is determined by considering the surface mineralogical composition, surface area, and site density. The number of surface reactive /functional groups, γ (mol/L), is related to the site density, N_s (site/nm^2), as follows [36]:

$$\gamma = \frac{10^{18} S_{BET} m_{ads} N_s}{V N_A}, \tag{17}$$

where S_{BET} is the Brunauer-Emmett-Teller surface area (m^2/g), m_{ads} is the mass of the adsorbent (g), V is the solution volume (L), and N_A is Avogadro's number. It is essential to mention that the carbonate surface area is 1.7 m^2/g, and its surface density is 5 sites per nm^2 [43]. At in-situ reservoir conditions, the formation fluid is in equilibrium with the surface of the reservoir rock and certain species get adsorbed on the surface of the rock. Thus, with the injection of low-salinity water, the saturation of water increases, and a certain portion of the reservoir rock surface comes in the contact with the injected water and the remaining reservoir rock surface remains unchanged. Thus, the concentration of adsorbed species is given by the following equation:

$$C_{a=} S_{bet} T_s (\alpha_r \beta_r + (1 - \alpha_r)\beta_r), \tag{18}$$

where α_r represents the fraction of the surface on which the adsorption process took place and β_r stands for the composition of adsorbed species unchanged on the *1-*α_r of surface fractions.

3. Model Validation

3.1. Zeta Potential Validation Studies

We validated the developed model using the surface complexation against the experimental data (zeta potential) provided in the literature. It is essential to mention that we investigated the change in zeta potential (carbonate and oil) with the variation in solution pH and matched the results with the zeta potential experimental (carbonate and oil) data.

3.1.1. Zeta-Potential: Carbonate

To evaluate the variation of zeta potential on the carbonate surface, where the carbonate surface is bounded by the reservoir brine. The various surface complexation reactions provided only in **Table 1** are used for validation because the model is validated for a pure calcite mineral. The results of the developed model with surface complexation and zeta potential experimental measurements performed by Thompson and Pownall [44] are shown in **Fig. 2(a)**. The said experimental setup was performed for the carbonates and it was brought to equilibrium at 25 °C with a 0.005 NaCl solution. They utilized NaOH to alter the pH of the solution. We adjusted the calcite Log K_{int} values to incorporate the temperature correction in the previous section. It is evident from the results depicted in **Fig. 2(a)** that the results of the developed model are in excellent agreement with the experimental data, where with the increase in solution pH the zeta potential also becomes negative. Moreover, initially, we tuned the surface area and site density; but this approach had a trivial effect. Then, we slightly modified the log K_{int} values and thus we successfully matched the

experimental data as shown in **Fig. 2(a)**. This approach of tuning log K_{int} values was recently suggested by [42] and [45]. It is worthy to mention that we considered the dissolution/precipitation reactions in matching the experimental data.

3.1.2. Zeta Potential: Oil

We utilized the experimental data performed by Buckley *et al.* [46] to confirm the oil-brine surface complexation model. They determined the zeta potential measurements at 25 ºC by using crude oil (4 ml) in 100 ml of 0.1 M NaCl solution. It is imperative to mention that the surface charge becomes negative, for oils with a low ratio of total oil base numbers (TBN) to total oil acid numbers (TAN). Moreover, for oils with high TBN/TAN values, this ratio becomes zero at high pH values [47]. Additionally, to estimate the zeta-potential at the oil-brine interface. We considered both groups: acid (carboxylic acid) and base (nitrogen base) along with their respective SCR as shown in **Table 2**. The Log K_{int} value for these SCRs was tuned to match the experimental data as shown in **Fig. 2(b)** and it shows that our developed model is in good agreement with experimentally determined zeta potential data. Furthermore, our results show that the surface charge of the crude oil decreases with the increase in pH.

3.2. Carbonate Corefloods: Simulation and Validation

To validate and prove the efficiency of our developed model, a detailed history matching is performed with the experimental data and effluent concentration of PDIs such as calcium, magnesium, and sulfate. These ions are known as potential determining ions because of their ability to adsorb on the carbonate surface and change its surface charge/potential [14]. As was previously mentioned, the experimental results of Shehata *et al.* [29] were used in this study. The experimental work of Shehata *et al.* [29] was selected because they performed several low salinity waterflooding experiments at 90 °C on Indiana limestone cores with 99.9% calcite and 0.1 % iron as HFO. The surface complexation reaction for the HFO is depicted in **Table 3.** In this study, the simulator ran for a pre-determined pore volume and the reservoir parameters were modified accordingly. Then, the calculations were performed assuming that the rock contains traces of ankerite/ferroan-dolomite [$Ca(Fe, Mg)(CO_3)_2$], siderite, dolomite, mica as biotite [$K(Mg,Fe)_3AlSi_3O_{10}(OH)_2$] and K-mica [$KAl_3Si_3O_{10}(OH)_2$], and alunite [$KAl_3(SO_4)_2(OH)_6$]. The formation water contains 0.001 mol/L of sulfate, thus determining the source of sulfate in formation water. It is assumed that the primary source of SO_4^{-2} is likely to be anhydrite because the kinetic dissolution of anhydrite-containing minerals releases SO_4^{-2}. The low level of anhydrite in the simulation model and its absence from XRD data is consistent with previous observations that reported that the low anhydrite concentrations fell below the detection limit of XRD [28 and [48].

We performed a detailed sensitivity analysis for the remaining 1% solid species in composition and found a good match with Ankerite (0.5%) and Anhydrite (0.5%) using the llnl.dat database in the Phreeqc simulator. In their coreflooding experiments, they injected 4.78 PVs of seawater at irreducible water saturation conditions, followed by 3.1 PV deionized water, and then, 4.1 PV of seawater (50 times diluted) injection. **Table 4** presents the detailed ionic compositions of formation water, seawater, and various diluted waters. The list of different reservoir rock properties used in the sensitivity analysis is shown in **Table 5**.

The total site density for the calcite surface used in the study is 5 sites/nm^2. This study used surface complexation reactions as previously presented in **Tables 1-3.** The acid and base numbers measured by Shehata *et al.* [29] are utilized to determine the number of sites in the oil-brine interface. Equations (16) and (17) were used to convert the acid and base numbers to sites/nm^2, respectively. It should be noted that the oil-specific surface area was assumed to be 1 g/m^2 according to Korrani and Jerauld [18]. The equations used to convert TAN and TBN to site/nm^2 are as follows:

$$\frac{Sites}{nm^2} = \frac{0.6022\times10^6\times\text{TAN(mgKOH/g oil)}\times\text{Oil specific area}(\frac{g\ oil}{m^2})}{1000Mw_{KOH}}, \quad (16)$$

$$\frac{Sites}{nm^2} = \frac{0.6022\times10^6\times\text{TBN(mgKOH/g oil)}\times\text{Oil specific area}(\frac{g\ oil}{m^2})}{1000Mw_{KOH}}. \quad (17)$$

To match the experimental data of Shehata *et al.* [29], we performed a sensitivity analysis of the equilibrium constant of the Brady and Thyne [40] base group surface complexation, Equation (18), as shown in **Table 3** from -5.0 to -1.8.

$$\text{-COOH} \leftrightarrow \text{-COO-} + \text{H+}, \qquad \log K_{25°C} = -1.8\ . \quad (18)$$

Moreover, the equilibrium constant of calcium and carboxylic surface complexation, Equation (19), was modified from -2.6 to -3.8.

$$\text{-COOH} + Mg^{2+} \leftrightarrow \text{-COOMg}^{+} + H^{+}, \qquad \log K_{25°C} = -3.8. \quad (19)$$

The value of Log K_{int} for the above-mentioned SCRs was used as a tuning parameter and temperature corrected values are given in **Table 3**. We tuned the calcite surface area and its site density. However, they have a trivial effect on matching the experimental data. Thus we modified the log K_{int} values recently proposed by Rego et al. [45], and Khurshid and Al-Shalabi [42] to match the experimental data. Thus, it can be observed from **Fig. 3** for Ca^{2+}, Mg^{2+}, and SO_4^{2-} ions that the results predicted by our developed model are in excellent agreement with the experimental data. It can be noticed from the results, we obtained a very good match for Ca^{2+} and Mg^{2+} ions except that of SO_4^{2-} ion. The noticeable difference in matching SO_4^{2-} ion is due to the quality of experimental data. Thus, a delay of sulfate ions in effluent concentration can be expected, but a delay of 2 PVs is too much to be considered as a result of adsorption as shown in **Fig. 3(c)**. Therefore, these results show that our developed model (with the incorporated surface complexation reactions) is efficient and offers the necessary understanding of the adsorption and desorption characteristics of the chemical species, the effect of pH variation, surface charge change alteration, and the concentration of surface species are the mechanism behind wettability alteration during engineered water injection.

4. Results and Discussion

Different factors that might affect the adsorption of aqueous species were analyzed with the developed model. The adsorption of divalent ions (Ca^{2+}, Mg^{2+}, and SO_4^{2-}) were predicted along with different parameters including ionic strength, reservoir temperature, sulfate-spiked injection water, and sulfate-diluted injection water. The composition of different water and rock properties are shown in **Tables 4** and **5**, respectively. The final composition of Indiana limestone, determined by simulations, along with dissolution kinetic parameters is 99% calcite, 0.5% ankerite, and 0.5% anhydrite. The average compositional surface area, $S=\Sigma\omega_i.s_i$ (ω is a mass fraction and s is mineral surface area) is 1.27 m^2/g, which agrees with the measured BET surface area of 1.25 m^2/g by Tagavifar *et al.* [36].

Ionic strength Effect. The effect of ionic strength of seawater, deionized water, and 50 times diluted seawater on the adsorption of Ca^{2+}, Mg^{2+}, and SO_4^{2-} was analyzed at 90 °C as shown in **Fig. 4**. The geochemical reactions and reservoir conditions remained the same as listed in **Tables 1 - 5**. The ionic strength of seawater, deionized water, and 50 times diluted water are 1.093, 6.345×10^{-7}, and 0.024 mol/kgw, respectively. **Fig. 4(a)** shows that the adsorption of calcium ions increases exponentially for seawater from 0.069 mg/g to 2.81 mg/g; however, for deionized water and 50 times diluted water, there is a slight increase in the adsorption of calcium ions. The adsorption behavior of magnesium is shown in **Fig. 4(b)**. It is apparent that by the injection of seawater the adsorption of magnesium increases from 2.88×10^{-4} mg/g to 7.8×10^{-2} mg/g, but it decreases for deionized water because of its zero ionic strength, and then, increases 50 times diluted seawater as its ionic strength is 0.55. Thus, the adsorption of magnesium is controlled by the ionic strength of the injected solution, with the increase in ionic strength, its adsorption increases and vice versa. The adsorption of sulfate, as shown in **Fig. 4(c)**, increases from 1.41×10^{-5} to 4.94×10^{-3} mg/g for seawater, followed by a further increase with deionized water from 4.94×10^{-3} to 1.32×10^{-2} mg/g. However, it decreases with 50 times

diluted seawater from 1.32×10^{-2} to 6.53×10^{-3} mg/g. Our results and finding shows that this phenomenon of adsorption for different ions at a different ionic strength of injected solutions is different and it could be due to:

i. With the decrease in ionic strength, the adsorption sites for calcium become inactive leading to an insignificant change in adsorption/desorption of calcium. However, the adsorption/desorption of magnesium and sulfate becomes active with the decrease in ionic strength due to the formation of electrical double layer complexes.
ii. The ionic strength of the injected solution is influenced by the activity coefficient of metallic ions and thus, it limits the transfer to the surface.

Temperature Effect. The injected water temperature effect is investigated in this subsection. **Fig. 5** shows the adsorption of calcium, magnesium, and sulfate ions at 90, 100, 110, and 120 °C. The adsorption of PDIs was analyzed at different temperatures during seawater, deionized water, and 50 times diluted water. The compositions of various waters can be found in **Table 4**.

It was observed that with the increase in temperature, the adsorption of calcium ions increases as shown in **Fig. 5(a)** only for the seawater injection cycle; however, calcium adsorption was not affected during deionized water and 50 times diluted water cycles. For the effect of temperature on the adsorption of magnesium, no major effect was pronounced during the seawater injection cycle. However, during the injection of deionized water, its adsorption decreases exponentially for all temperatures except for 90 °C as shown in **Fig. 5(b)**. Afterward, as soon as 50 times diluted seawater water is injected, the adsorption of magnesium increases due to an increase in the concentration of magnesium in the reservoir. One can note that the adsorption of magnesium decreased with temperature increase mainly during deionized water and 50 times diluted water cycles.

Fig. 5(c) depicts the behavior of sulfate ion adsorption in the reservoir as a function of temperature. It can be observed that the adsorption of sulfate decreases with the increase in temperature during seawater injection. However, the adsorption of sulfate starts increasing with the increase in temperature in deionized water injection. Moreover, during the injection of diluted seawater (50 times), the adsorption of sulfate decreases with an insignificant effect on temperature. Thus, with a decrease in ionic strength (from seawater to deionized water), the amount of adsorption of PDIs increases with the increase in temperature as shown in **Fig 5 (a) and (c)** for calcium and sulfate. It happens because the adsorbent sites become more active at a higher temperature for calcium and sulfate, and vice versa for magnesium as shown in **Fig. 5(b)**.

Sulfate Spiking Effect. The effect of sulfate spiking on the adsorption of calcium ions at 90 °C is shown in **Fig. 6(a)**. It can be observed that with sulfate spiking the adsorption of calcium was not affected and it remained the same in the 2nd cycle for both deionized water and sulfate-spiked water. The effect of sulfate spiking on the adsorption of magnesium is shown in **Fig. 6(b)**. It is evident from this figure that the adsorption of magnesium increases with the injection of sulfate-spiked water as opposed to deionized water. On the contrary, **Fig. 6(c)** shows that with the injection of sulfate-spiked water, the adsorption of sulfate decreases when compared to that of deionized water. These results show that high-temperature sulfate and magnesium are active and calcium is in/less active that why calcium adsorption is not affected by the injection of deionized and sulfate-spiked water. These findings are also mentioned by Al-Shalabi and Sepehrnoori [2].

Sulfate Dilution Effect. **Fig. 6(a)** depicts the effect of sulfate dilution on the adsorption of calcium ions at 90 °C. It can be observed that with the sulfate dilution, the adsorption of calcium was not affected and it remained the same in the 2nd cycle similar to that of deionized water. The effect of sulfate dilution on the adsorption of magnesium is shown in **Fig. 6(b)**. It is evident from this figure that with the injection of diluted sulfate, the adsorption of magnesium has increased compared to that of deionized water. The opposite was observed for the sulfate ion as shown in **Fig. 6(c)** where the injection of diluted sulfate brine decreased sulfate adsorption as opposed to deionized water. These findings show that the adsorption of sulfate is controlled by the composition of injected water.

***Comparison of Various Waters on Surface Charge and pH*. Fig. 7(a) and (b)** show the effect of various waters such as deionized water, diluted sulfate water, and spiked sulfate water on surface charge and pH, respectively. It is evident from **Fig. 7(a)** that deionized water is the most successful water injection recipe in decreasing the surface charge of the carbonate rock in the selected case study followed by the injection of spiked sulfate and diluted sulfate. It is important to mention that spiked sulfate and diluted sulfate have the same trends in the adsorption of calcium, magnesium, and sulfate as shown in **Fig. 6**. However, the analysis of surface charge revealed that spiked sulfate water injection decreases the surface charge more than the diluted sulfate water. Thus, the spiked sulfate water performed better than the diluted sulfate water injection, at the same time the results show that the deionized water is the most successful scenario in recovering oil from the selected case study.

5. Ion Adsorption Mechanism: EWI in Carbonates

In carbonates, the alteration of reservoir wettability is considered to be the main mechanism underlying additional oil recovery by LSW/EWI. Yousef *et al.* [13] executed several experiments on carbonates and measured contact angles. They measured the contact angle with formation water, seawater, and various diluted seawater. They found that two tests (tests 2 & 3) have a major drop in contact angle by seawater and its various diluted recipes. Thus, our adsorption modeling results, discussed in the previous section, prove that during seawater injection, the adsorption of Ca^{2+}, Mg^{2+}, and SO_4^{2-} could have led to the observed oil recovery by Shehata *et al.* [29]. This further verifies that the injection of regular seawater can change the wettability of a reservoir from a hydrophobic (oil-wet) to a hydrophilic (water-wet) state. We used the results obtained from utilizing the surface complexation reactions and determined the effect of different ions that contributed to the alteration of carbonate wettability. From the surface complexation modeling, it is observed that most probably the mechanism underlying the increase in oil recovery and respective wettability modification in Shehata *et al.* [29] is due to the adsorption and desorption of all potential determining ions (Ca^{2+}, Mg^{2+}, and SO_4^{2-}) as shown in **Fig. 8**.

The adsorption and desorption of potential determining ions that lead to the decrease in surface charge is the governing process of wettability alteration in this specific case. This finding is established by the concentration of different ionic species in the effluent. Thus, we correlated the calcium, magnesium, and sulfate ions concentration in the effluent with additional oil recovery. It is evident from **Fig. 8** that for seawater, deionized water, and 50 times diluted seawater injection. The adsorption and desorption of PDIs decreased the surface charge of carbonate rock as shown in **Fig. 7(a)**, leading to maximum incremental oil recovery at the injection of different waters as shown in **Fig. 8**. This alteration of carbonate surface charge would occur when the point of zero charges is exceeded as mentioned by Al-Shalabi *et al*., [15]. This point of zero charges is around 9.2 for calcite and 7.4 for dolomite as proposed by Gupta and Mohanty [49]. Moreover, in carbonates, this point of zero charges depends on pH variation, the concentration of PDIs, and the composition of injected water. Additionally, Pokrovsky *et al.* [43] found that for calcite the point of zero charge ranges from 7 to 12, and for dolomite it lies in the range of 6 to 8.8. Furthermore, Lichaa *et al.* [50] used deionized water for carbonate core containing 40% calcite and 60% dolomite. They observed that the point of zero charges lay in the range of 3.4 to 4.6. Alotaibi *et al*. [51] also conducted various experiments on calcite and dolomite and found that the point of zero charges of dolomite is less than that of calcites.

It is essential to mention that the Indiana limestone used by [29] is composed of 99% calcite, 0.5% anhydrite, and 0.5% ankerite. Thus, the increase in pH as shown in **Fig. 7(b),** and PDIs adsorption/desorption phenomena decreased the surface charge at the solid-water interface from 0.0037 to 0.00032 equivalents as shown in **Fig. 7(a)**, thus the wettability of the reservoir is modified from oil-wet to more water-wet state. Thus, the increase in pH and decrease in surface charge as shown in **Fig. 7(a) and (b)**, lead to the force of repulsion between the solid/water interfaces. Thus, the water film is stabilized by the force of repulsion that expands the electrical double layer and thus renders the rock more water-wet. The results show that this electrical double layer is created and supported by the adsorption and desorption of PDIs.

Therefore, based on the detailed surface complexation modeling, a chemical mechanism (adsorption and desorption of PDIs, decrease in rock surface charge, and pH increase) is a suggested mechanism underlying wettability alteration. The change in adsorption/desorption of SO_4^{2-}, $Ca^{+2,}$ and Mg^{+2}, increase pH number and decreases surface charge. Thus, Ca^{+2} and Mg^{+2} may react with the carboxylic acid group forms a complex (get adsorbed), and release oil from the carbonate surface. Therefore, the recovery of oil is not only a function of change in pH as revealed by Al-Shalabi *et al.* [15], but it is a combination of PDIs adsorption/desorption, and a decrease in rock surface charge. It is important to mention that these findings cannot be generalized because seawater injection-related recovery of oil is subject to reservoir thermodynamics conditions (temperature and pressure), the composition of reservoir rock, crude-oil acid, and base number, and the composition of seawater.

6. Summary and Conclusions

This study aimed to characterize the efficiency of ionic adsorption/desorption, change in surface charge, and pH, as the mechanism of altering wettability in carbonates during low salinity/engineered water injection (LSWI/EWI). The experimental work of Shehata *et al.* [29], Thompson and Pownall [44], and Buckley *et al*. [46] were used to validate the proposed surface complexation model using the Phreeqc. The main findings of this work can be summarized as follows:

- The developed surface complexation-based adsorption/desorption model determines for the first time the adsorption/desorption level of various potential determining ions.
- We utilized fluid and rock properties including XRD data, and oil acid and base numbers to best capture the rock/brine/crude oil interactions in the developed model and their overall effect on the wettability of the selected carbonate surface.
- It is found that calcite is the main mineral in the rock composition that is affecting surface charge, ions adsorption, and desorption.
- It is observed that the adsorption of ionic species depends on ionic strength and species activity, where calcium adsorption remained constant while magnesium and sulfate adsorptions varied with the ionic strength.
- The magnesium ions were found to be the most sensitive potential determining ion to temperature as opposed to calcium and sulfate ions.
- The sulfate spiking and dilution of injected low salinity/engineered water lead to a decrease in sulfate adsorption since the sulfate starts reacting with magnesium and forming complexes.
- We found that the adsorption/desorption of potential determining ions, decrease in surface charge, and increase in pH during EWI are the responsible mechanisms for wettability alteration and the related incremental oil recovery for the investigated study.

Limitations and Future work

The limitation of this study is that it didn't use the coupled two-phase flow simulator. However, in this study, we used the oil surface complexation reactions to include the effect of the oil phase in the porous media during low salinity/engineered water injection and the respective geochemical interactions. It is important to mention that the use of the employed oil-based surface complexation reactions assisted in capturing the effect of acid and base groups (carboxylic acid and nitrogen base) present in the oil. Therefore, the proposed approach facilitated to reveal the factors affecting the adsorption/desorption of ionic species at the rock-oil-water interface during low salinity/engineered water injection (LSWI/EWI). Thus, the suggested approach can be utilized in reservoir simulators to estimate the recovery of oil due to wettability alteration during low salinity/engineered water injection (LSWI/EWI) in carbonates, which will be investigated in our future work. Moreover, the low salinity/engineered water injection (LSWI/EWI) and the respective oil recovery vary from case to case, and hence, the findings cannot be generalized.

Acknowledgments

The authors wish to acknowledge Khalifa University of Science and Technology for funding this research. This publication is based upon work supported by the Khalifa University of Science and Technology under Award No. [8474000240].

References

1. Sheng, J. J., 2011, "Modern Chemical Enhanced Oil Recovery - Theory and Practice," Gulf Professional Publishing, Elsevier, 1st Edition, pp. 100-250, ISBN 9781856177450, https://doi.org/10.1016/B978-1-85617-745-0.00018-8.,
2. Al-Shalabi, E. W. and Sepehrnoori, K., 2017, "*Low Salinity and Engineered Water Injection for Sandstone and Carbonate Reservoirs,"* Gulf Professional Publishing, Elsevier, 1st Edition, pp. 178, ISBN: 978-0-12-813604-1, Cambridge, USA.
3. Khurshid, I., Al-Shalabi, E.W, Afgan, I., Al-Attar. 2021, "A Numerical Approach to Investigate the Impact of Acid-Asphaltene Sludge Formation on Wormholing during Carbonate Acidizing," *J. Energy Resour. Technol.,* https://doi.org/10.1115/1.4051738.
4. Khurshid, I., Fujii, Y., and Choe, J., 2015, "Analytical Model to Determine Optimal Fluid Injection Time Ranges for Increasing Fluid Storage and Oil Recovery: A Reservoir Compaction Approach," *J. Pet. Sci. Eng.*, 135, pp. 240-245.
5. Buckley, J. and Liu, Y., 1998, "Some Mechanisms of Crude Oil/Brine/Solid Interactions. *J. Pet. Sci. Eng.*, 20(3), pp. 155−160.
6. Standnes, D. C. and Austad, T., 2003, "Wettability Alteration in Carbonates: Interaction between Cationic Surfactant and Carboxylates as a Key Factor in Wettability Alteration from Oil-Wet to Water-Wet Condition," *Colloid Sur. A-Physicochem. Eng. Asp.,* 216(1-3), pp. 243−259.
7. Tang, G. and Morrow, N., 1999, "Influence of Brine Composition and Fines Migration on Crude Oil/Brine/Rock Interactions and Oil Recovery," *J. Pet. Sci. Eng.*, 24(2–4), pp. 99–111.
8. Høgnesen, E., Strand, S., and Austad, T., 2005, "Waterflooding of Preferential Oil-Wet Carbonates: Oil Recovery Related to Reservoir Temperature and Brine Composition," Paper SPE 94166, *67th SPE Europec/EAGE Annual Conference,* Madrid, Spain.
9. Zhang, P. M. and Austad, T., 2006, "Wettability and Oil Recovery from Carbonates: Effects of Temperature and Potential Determining Ions," *Colloid Sur. A-Physicochem. Eng. Asp.,* 279, pp. 179−187.
10. Zhang, P. M., Tweheyo, M. T., and Austad, T., 2007, "Wettability Alteration and Improved Oil Recovery by Spontaneous Imbibition of Seawater into Chalk: Impact of Potential Determining Ions Ca^{2+}, Mg^{2+}, and SO_4^{2-}," *Colloid Sur. A-Physicochem. Eng. Asp.,* 301, pp. 199−208.
11. Puntervold, T., Strand, S., and Austad, T., 2009, "Co-injection of Seawater and Produced Water to Improve Oil Recovery from Fractured North Sea Chalk Oil Reservoirs," *Energy & Fuels*, 23(5), pp. 2527−2536.
12. Hiorth, A., Cathles, L. M., and Madland, M. V., 2010, "The Impact of Pore Water Chemistry on Carbonate Surface Charge and Oil Wettability," *Transp. Porous Media*, 85(1), pp. 1−21.
13. Yousef, A. A., Al-Saleh, A., Al-Kaabi, A., and Al-Jawfi, M., 2011, "Laboratory Investigation of the Impact of Injection-Water Salinity and Ionic Content on Oil Recovery from Carbonate Reservoirs," *SPE Reserv. Evaluation Eng.,* 14, pp. 578−593.
14. Austad, T., Shariatpanahi, S., Strand, S., Black, C., and Webb, K., 2012, "Conditions for a Low-salinity Enhanced Oil Recovery (EOR) Effect in Carbonate Oil Reservoirs," *Energy & Fuels*, 26(1), pp. 569−575.
15. Al-Shalabi, E. W., Sepehrnoori, K., and Pope, G., 2015, "Geochemical Interpretation of Low-Salinity-Water Injection in Carbonates in Oil Reservoirs," Paper SPE 169101, *SPE J.,* 20(6), pp. 1212-1226.
16. AlHammadi, M., Mahzari,P. Sohrabi M., 2018, "Fundamental investigation of underlying mechanisms behind improved oil recovery by low salinity water injection in carbonate rocks," *Fuel,* 220, pp. 345-357. 10.1016/j.fuel.2018.01.136
17. Mahani, H., Keya, A. L., Berg, S., and Nasralla, R., 2017, "Electrokinetics of Carbonate/Brine Interface in Low-Salinity Waterflooding: Effect of Brine Salinity, Composition, Rock Type, and pH on ζ-Potential and a Surface-Complexation Model," *SPE J.*, 22(1), pp. 53-68.
18. Korrani, A. K. N. and Jerauld, G. R., 2019, "Modeling Wettability Change in Sandstones and Carbonates using a Surface-Complexation-Based Method," *J. Pet. Sci. Eng.*, 174, pp. 1093-1112.
19. Khurshid, I., Al-Shalabi, E. W., and Alameri, W., 2020, "Influence of Water Composition on Formation Damage and Related Oil Recovery in Carbonates: A Geochemical Study," *J. Pet. Sci. Eng.*, 107715, 195, pp. 1-21.
20. Folk, R. L., 1959, "Practical Petrographic Classification of Limestones," *AAPG Bulletin*, 43(1), pp. 1–38.
21. Levitt, D. B., Weatherl, R. K., Harris, H. W., McNeil, R. I., Didier, M., Loriau, M., Gaucher, E. C., and Bourrel, M., 2015, "Adsorption of EOR Chemicals under Laboratory and Reservoir Conditions, Part 1-Iron Abundance and Oxidation State," *IOR 2015-18th European Symposium on Improved Oil Recovery*.
22. Kosmulski, M., 2002, "The pH-Dependent Surface Charging and the Points of Zero Charge," *J. Colloid Interface Sci.,* 253(1), pp. 77–87.

23. Stumm, W. and Morgan, J. J., 1996, "*Aquatic Chemistry: Chemical Equilibria and Rates in Natural Waters*," John Wiley & Sons, 3rd Edition, ISBN: 978-0-471-51185-4.
24. Na, C., Kendall, T. A., and Martin, S. T., 2007, "Surface-potential Heterogeneity of Reacted Calcite and Rhodochrosite," *Environ. Sci. Technol.*, 41(18), pp. 6491–6497.
25. Nwidee, L. N., Lebedev, M., Barifcani, A., Sarmadivaleh, M., and Iglauer, S., 2017, "Wettability Alteration of Oil-wet Limestone Using Surfactant-Nanoparticle Formulation," *J. Colloid Interface Sci.*, 504(15), pp. 334–345.
26. Pham, T. D., Kobayashi, M., and Adachi, Y., 2015, "Adsorption of Anionic Surfactant Sodium Dodecyl Sulfate onto Alpha Alumina with Small Surface Area," *Colloid Polym. Sci.*, 293(1), pp. 217–227.
27. Southwick, J. G., Pol, E. V. D., Rijn, C. H. V., Batenburg, D. W. V., Boersma, D., Svec, Y., Mastan, A. A., Shahin, G., and Raney, K., 2016, "Ammonia as alkali for alkaline/surfactant/polymer floods," *SPE J.*, 21(1), pp. 10–21.
28. Levitt, D. and Bourrel, M., 2016, "Adsorption of EOR Chemicals under Laboratory and Reservoir Conditions Part III: Chemical Treatment Methods," Paper SPE 179636, *SPE Improved Oil Recovery Conference*, Tulsa USA.
29. Shehata, A. M., Alotaibi, M. B., and Nasr-El-Din, H. A., 2014, "Waterflooding in Carbonate Reservoirs: Does the Salinity Matter?," *SPE Reserv. Evaluation Eng.* 17(3), pp. 304-313.
30. Parkhurst, D. L., and Appelo, C. A. J., 2013, "Description of Input and Examples for PHREEQC Version 3–*A Computer Program for Speciation, Batch-reaction, One-dimensional Transport, and Inverse Geo-chemical Calculations*," In US Geological Survey Techniques and Methods, Section A: Groundwater, Book 6: Modeling Techniques, Chap. 43. Denver: US Geological Survey.
31. Jackson M.D., Vinogradov, J., Hamon, G., and Chamerois, M., 2016, "Evidence, Mechanisms and Improved Understanding of Controlled Salinity Water Flooding Part 1: Sandstones," *Fuel*, 185, pp. 772–93.
32. Wang, X. and Alvarado, V., 2017, "Effects of Low-Salinity Water Flooding on Capillary Pressure Hysteresis," *Fuel*, 207, pp. 336–343.
33. Hirasaki, G., 1991, "Wettability: Fundamentals and Surface Forces," *SPE Format. Evaluation*, 6(2), pp. 217−226.
34. Xie, Q., Saeedi, A., Pooryousefy, E., and Liu, Y., 2016, "Extended DLVO-based Estimates of Surface Force in Low Salinity Water Flooding," *J. Mol. Liq.*, 221, pp. 658–665.
35. Morse, J. W., and Arvidson, R. S., 2002, "The Dissolution Kinetics of Major Sedimentary Carbonate Minerals," *Earth-Science Reviews*, 58(1-2), pp. 51-84.
36. Tagavifar, M., Sharma, H., Wang, D., Jang, S. H., and Pope, G., 2018, "Alkaline/Surfactant/Polymer Flooding with Sodium Hydroxide in Indiana Limestone: Analysis of Water/Rock Interactions and Surfactant Adsorption," *SPE J.*, 23(6), pp. 2279-2301.
37. Gandomkar, A. and Kharrat, R., 2013, "Anionic Surfactant Adsorption through Porous Media in Carbonate Cores: An Experimental Study," *Ener. Sour., Part A*, 35, pp. 58−65.
38. Pillai, P. and Mandal, A., 2019, "Wettability Modification and Adsorption Characteristics of Imidazole-Based Ionic Liquid on Carbonate Rock: Implication for Enhanced Oil Recovery," *Energy & Fuels*, 33, pp. 727-738.
39. Ahmadi, M. A., and Shadizadeh, S. R., 2015, "Experimental Investigation of a Natural Surfactant Adsorption on Shale-Sandstone Reservoir Rocks: Static and Dynamic Conditions," *Fuel*, 159, pp. 15−26.
40. Brady, P. V., and Thyne, G., 2016, "Functional Wettability in Carbonate Reservoir," *Energy & Fuels*, 30, pp. 9217-9225.
41. Israelachvili, J., 2011, "Intermolecular and Surface Forces," Academic Press, Elsevier, 3rd Edition, ISBN: 978-0-12-375182-9.
42. Khurshid, I., Al-Shalabi. E., 2022, "New Insights into Modeling Disjoining Pressure and Wettability Alteration by Engineered Water: Surface Complexation based Rock Composition Study," *J. Pet. Sci. Eng.*, 208, pp. 109584.
43. Pokrovsky, O. S., Schott, J., and Thomas, F., 1996, "Dolomite Surface Speciation and Reactivity in Aquatic systems," *Geochim. Cosmochim. Acta*, 63, pp. 3133−3143.
44. Thompson, D. W., and Pownall, P. G., 1989, "Surface Electrical Properties of Calcite," *J. Colloid Interface Sci.*, 131(1): 74-82.
45. Rego, F. B., Mehrabi, M., Sanaei, A., and Sepehrnoori, K., 2021, "Improvements on Modelling Wettability Alteration by Engineered Water Injection: Surface Complexation at the Oil/Brine/Rock Contact," *Fuel*, 284, pp. 118991.
46. Buckley, J. S., Takamura, K., and Morrow, N. R., 1989, "Influence of Electrical Surface Charges on the Wetting Properties of Crude Oil," *SPE Reservoir Eng.*, 4: 332−340.
47. Dubey, S. T. and Doe, P. H., 1993, "Base Number and Wetting Properties of Crude Oils," *SPE Reservoir Eng.*, 8(3): 195-200.
48. Lopez-Salinas, J.L., Hirasaki, G. J., and Miller, C. A., 2011, "Determination of Anhydrite in Reservoirs for EOR," Paper SPE-141420, *SPE International Symposium on Oilfield Chemistry*, Woodland, Texas, USA.
49. Gupta, R. and Mohanty, K. K., 2010, "Wettability Alteration Mechanism for Oil Recovery from Fractured Carbonate Rocks," *Transp. Porous Media*, 87(2), pp. 635-652.
50. Lichaa, P. M., Alpustun, H., Abdul, J. H., Nofal, W. A., and Fuseni, A. B., 1993, "Wettability Evaluation of a Carbonate Reservoir Rock," *Proc. Advances in Core Evaluation III Reservoir Management, European Core Analysis Symposium*, p. 327.
51. Alotaibi, M. B., Nasr-El-Din, H. A., and Fletcher, J. J., 2011, "Electrokinetics of Limestone and Dolomite Rock Particles," Paper SPE 148701, *SPE Reserv. Evaluation Eng.*, 14(5), pp. 594-603.

644 **Table 1: Different calcite-based surface complexation reactions at the Calcite/Brine interface**

Chemical Reaction No.	Surface Complexation Geochemical Reactions	Log K_{int}				
		25 °C				90 °C
		Hiorth *et al.* [12]	Brady and Thyne [40]	Korrani and Jerauld [18]	Tuned Model	Temperature Adjusted Model
CB-1	$>CO_3H \leftrightarrow >CO_3^- + H^+$	-4.9	-5.1	-4.9	-5.1	-6.1
CB-2	$>CO_3H + Ca^{2+} \leftrightarrow >CO_3Ca^+ + H^+$	-3.16	-2.6	-1.74	-2.6	-2.7
CB-3	$>CO_3H + Mg^{2+} \leftrightarrow >CO_3Mg^+ + H^+$	-3.17	-2.6	-1.73	-2.6	-2.7
CB-4	$>CaOH + H^+ \leftrightarrow >CaOH_2^+$	12.9	11.85	12.9	11.5	11.33
CB-5	$>CaOH + HCO_3^- \leftrightarrow >CaCO_3^- + H_2O$	3.32	17.1	3.32	10.1	8.8
CB-6	$>CaOH_2^+ + SO_4^{2-} \leftrightarrow >CaSO_4^- + H_2O$	2.1	2.1	2.1	2.1	0.8

645
646
647 **Table 2: Different oil-based surface complexation reactions at the Oil/Brine interface**

Chemical Reaction No.	Surface Complexation Geochemical Reactions	Log K_{int}		
		25 °C		90 °C
		Brady and Thyne [40]	Tuned Model	Temperature Adjusted Model
OB-1	$-NH + H^+ \leftrightarrow -NH_2^+$	-6.0	-6.0	-7.3
OB-2	$-COOH \leftrightarrow -COO^- + H^+$	-5.0	-1.8	-2.0
OB-3	$-COOH + Ca^{2+} \leftrightarrow -COOCa^+ + H^+$	-3.8	-3.8	-3.9
OB-4	$-COOH + Mg^{2+} \leftrightarrow -COOMg^+ + H^+$	-2.6	-3.8	-3.9

648
649
650 **Table 3: Different iron oxide-based surface complexation reactions at Trace Minerals/Brine interface**

Chemical Reaction No.	Surface Complexation Geochemical Reactions	Log K_{int}		
		24 °C		90 °C
		Tagavifar *et al.* [36]	Tuned Model	Temperature Corrected Model
TM1	$>Fe(w)OH + H^+ \leftrightarrow >Fe(w)OH_2^+$	8.49	8.49	10.1
TM2	$>Fe(w)OH \leftrightarrow >Fe(w)O^- + H^+$	-9.1	-9.1	-9.2
TM3	$>Fe(s)OH + H^+ \leftrightarrow >Fe(s)OH_2^+$	8.49	8.49	8.4
TM4	$>Fe(s)OH \leftrightarrow >Fe(s)O^- + H_2^+$	-8.93	-8.93	-9.06
TM5	$>Fe(w)OH + Fe^{2+} \leftrightarrow >Fe(w)OFeOH + 2H^+$	-2.98	-2.98	-3.1
TM6	$>Fe(w)OH + Fe^{2+} + H_2O \leftrightarrow >Fe(w)OFe^+ + H^+$	-15.98	-15.98	-15.9
TM7	$>Fe(s)OH + Fe^{2+} \leftrightarrow >Fe(s)OFe^+ + H^+$	-0.98	-0.98	-1.1
TM8	$>Fe(w)OH + Ca^{2+} \leftrightarrow >Fe(w)OCa^+ + H^+$	-6.05	-6.05	-6.2
TM9	$>Fe(w)OH + Mg^{2+} \leftrightarrow >Fe(w)OMg^+ + H^+$	-6.8	-6.8	-6.9

651

652 **Table 4: Composition of formation water, seawater, and modified water [29]**

Salinity Unit		mol/L								mol/kgw	PPM	meq/ml	
Ionic Species		Ca^{2+}	Na^{+}	Cl^{-}	SO_4^{2-}	Mg^{2+}	HCO_3^{2-}	Ba^{2+}	Sr^{2+}	Ionic Strength	TDS	Anions	Cations
Field Formation Water		0.744	2.19	4.042	0.001	0.175	0.006	7.29×10^{-5}	0.012	6.443	229,218	4.05	4.05
Original Seawater		0.017	0.734	0.878	0.037	0.094	0.003	0	0	1.093	52,304	0.95	0.95
Modified Seawater	Two-Times Spiked Sulfate	0.017	0.814	0.878	0.074	0.094	0.003	0	0	1.109	60,071	1.03	1.03
	Two-Times Diluted Sulfate	0.017	0.704	0.878	0.019	0.094	0.003	0	0	1.05	52,206	0.92	0.92
	50-Times Diluted Seawater	3.31×10^{-4}	0.014	0.017	7.41×10^{-4}	1.88×10^{-3}	6.32×10^{-5}	0	0	0.024	1046	0.02	0.02

Table 5: Reservoir rock properties used for simulation [29]

Parameter	Value
Core Porosity, %	21.2
Core Brine Permeability, mD	176.6
Core Length, cm	15
Core Diameter, cm	3.8
Temperature, °C	90
Lithology, %	Calcite (99.9), Iron as HFO (0.1)
Elements/Pseudo-elements	Calcium, Sodium, Chloride, Magnesium, Sulfate, Carbonate, and Hydrogen
Solid Species	Calcite, and Fe-Dolomite
Gridblocks	20 × 1 × 1 (1D Model)
Diffusion Coefficient, m^2/s	0.0
Dispersivity, m	0.03
Timesteps, seconds	700
Direction of Flow	Forward
Boundary Conditions	Flux-flux

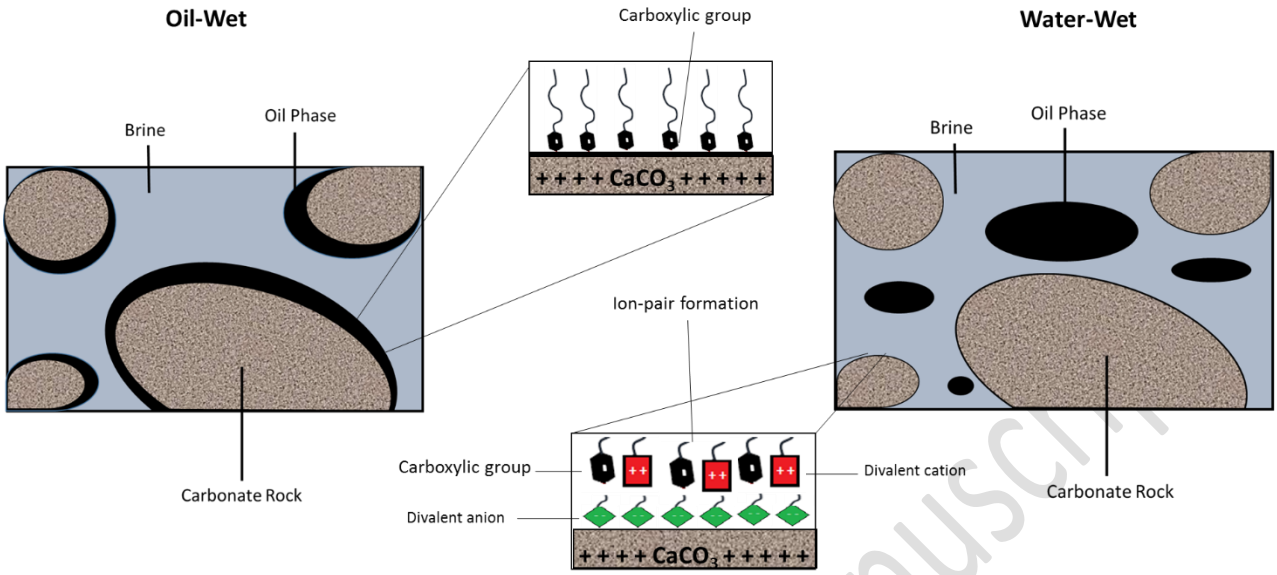

Fig. 1: Schematic diagram of wettability alteration in carbonates with ion adsorption of potential determining ions (Ca^{+2}. Mg^{+2}, SO_4^{-2})

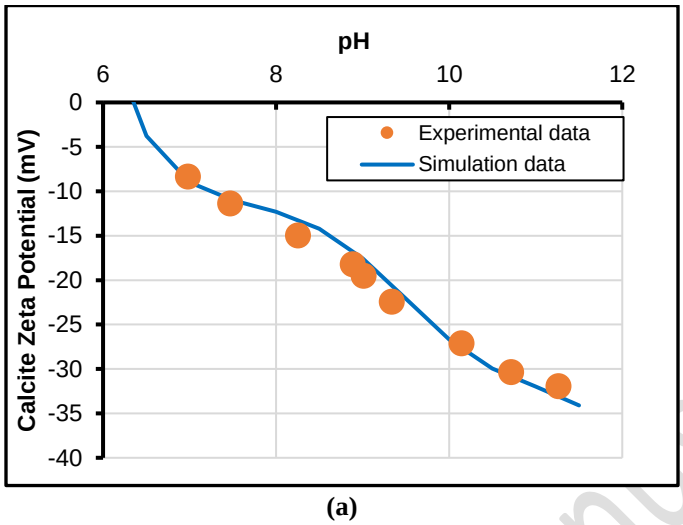

(a)

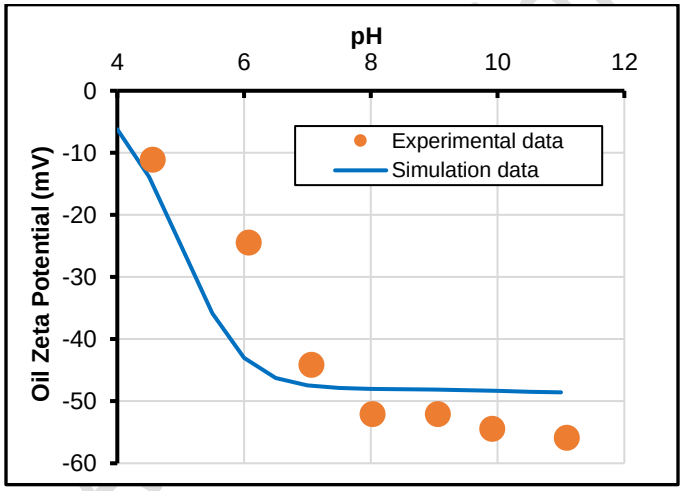

(b)

Fig. 2: Comparison of simulation data against experimental data for (a) pH results with experimental data at 25 ºC in 0.005 M NaCl, data from Thompson and Pownall, [44], (b) pH results with experimental data at 25 ºC in 0.1 M NaCl, data from Buckley *et al.*, [46].

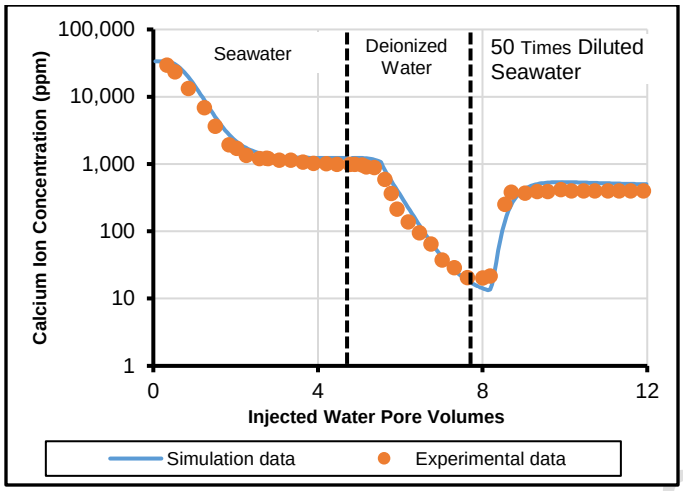

672
673

(a)

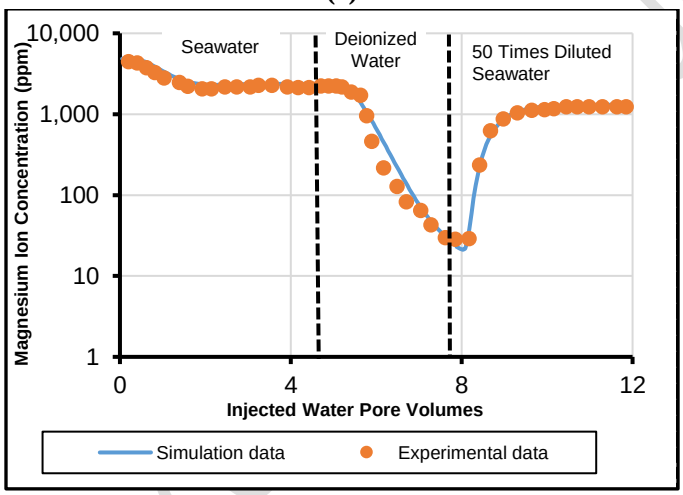

674
675

(b)

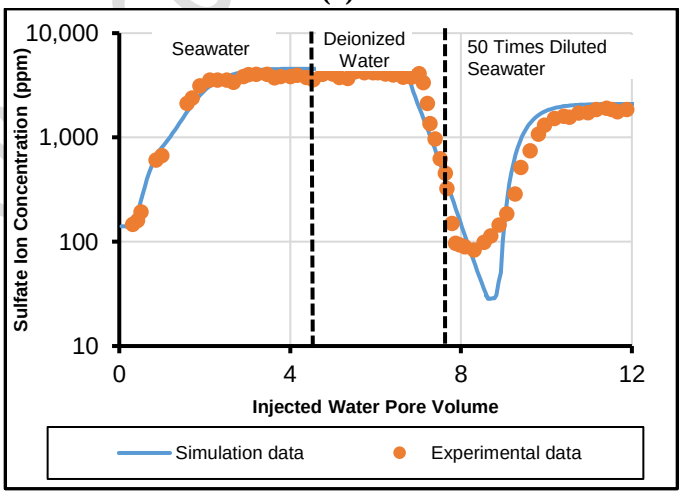

676
677

(c)

678 **Fig. 3: Comparison of simulation concentration data of different aqueous species with Shehata *et al.* [29]**
679 **experimental data at 90 °C for (a) Calcium ion, (b) Magnesium ion, and (c) Sulfate ion.**
680
681

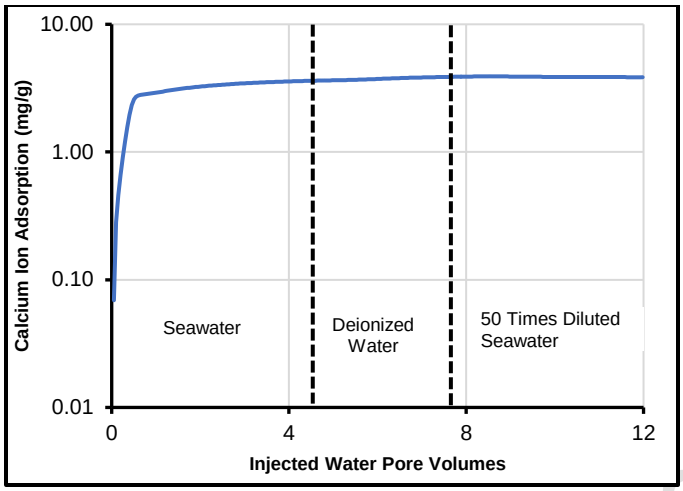

682
683

(a)

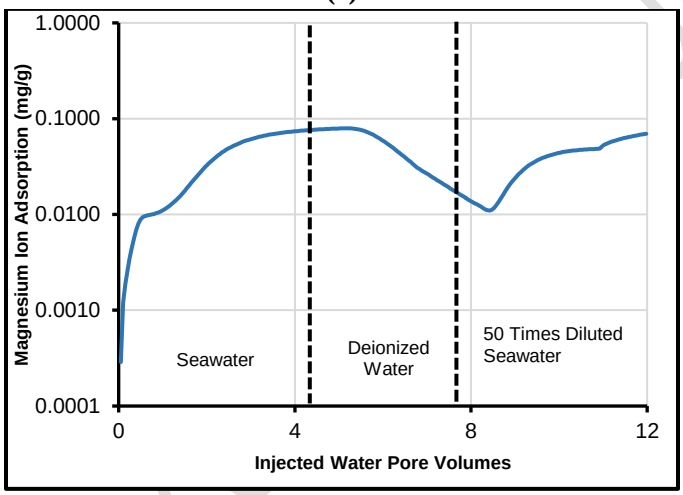

684
685

(b)

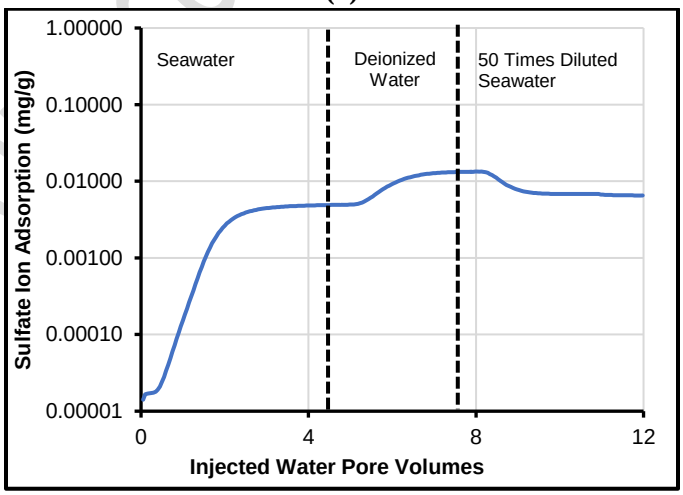

686
687

(c)

688 **Fig. 4: Effect of ionic strength on ion adsorption at 90 °C for (a) Calcium ion, (b) Magnesium ion, and (c)**
689 **Sulfate ion.**
690
691
692

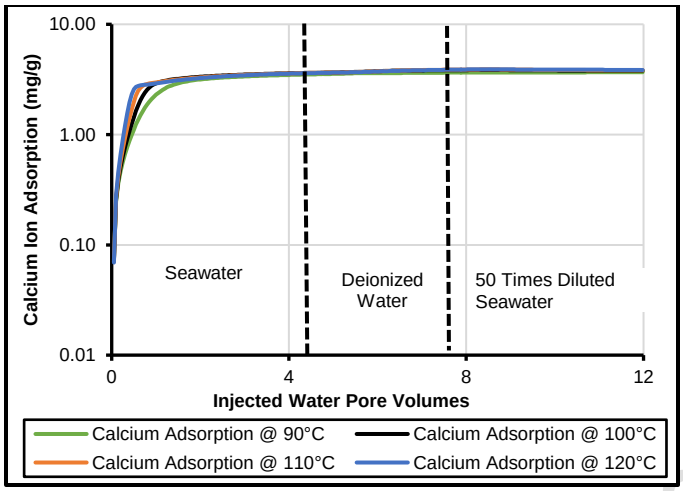

(a)

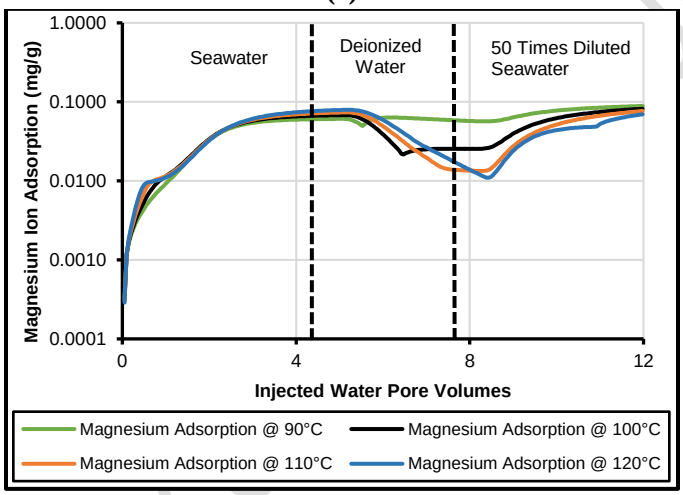

(b)

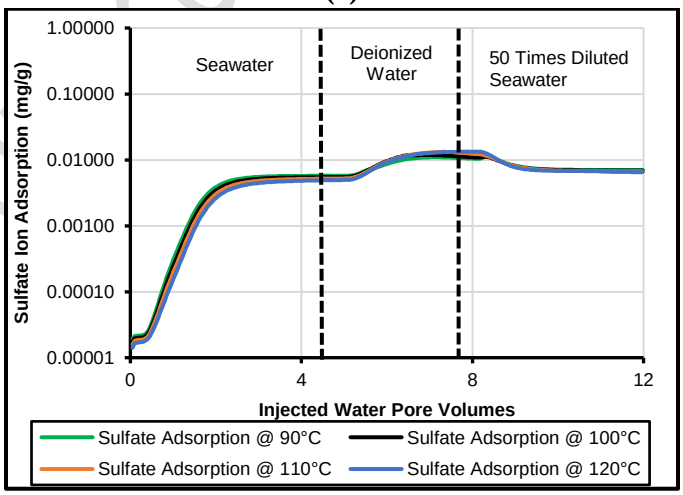

(c)

Fig. 5: Effect of temperature on ions adsorption for (a) Calcium ion, (b) Magnesium ion, and (c) Sulfate ion.

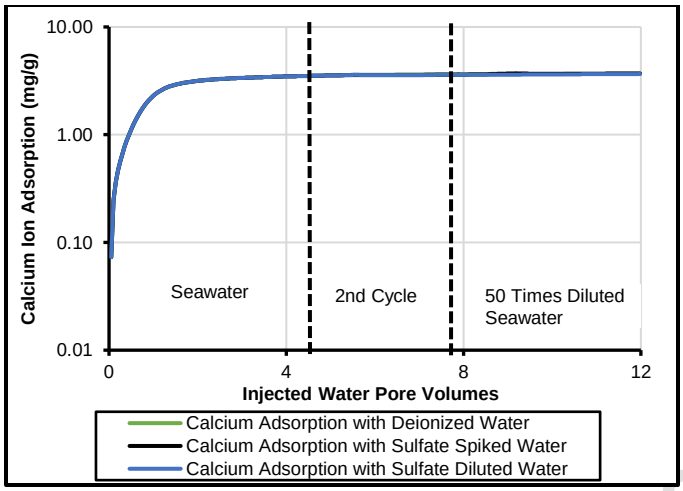

(a)

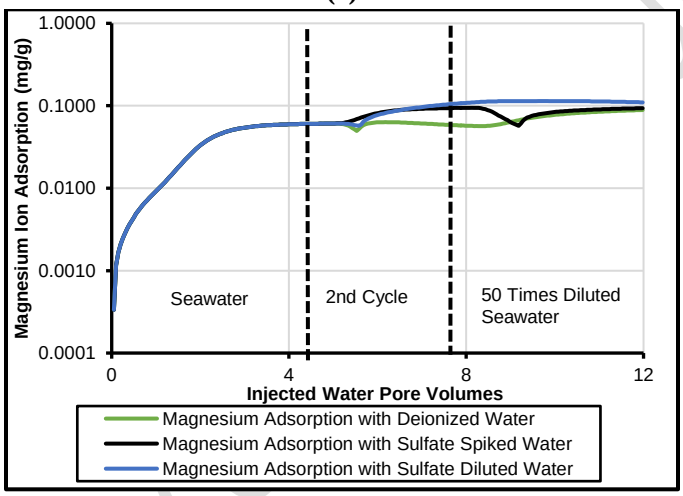

(b)

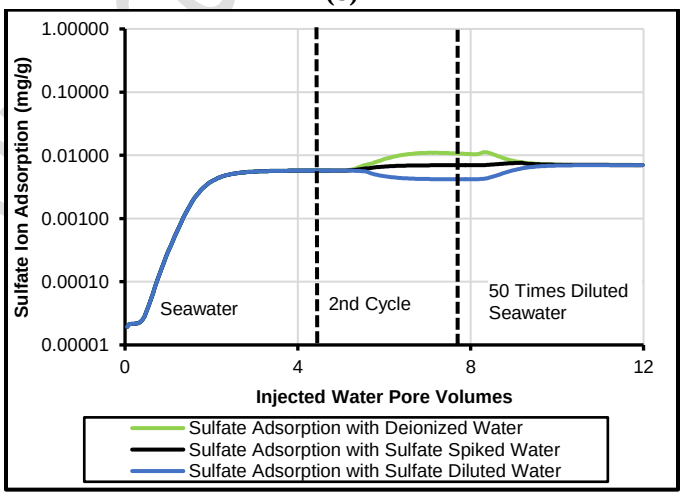

(c)

Fig. 6: Effect of different waters (Deionized, Sulfate Spiked, and Sulfate Diluted) on adsorption at 90 °C and 2nd cycle for (a) Calcium ion, (b) Magnesium ion, (c) Sulfate ion.

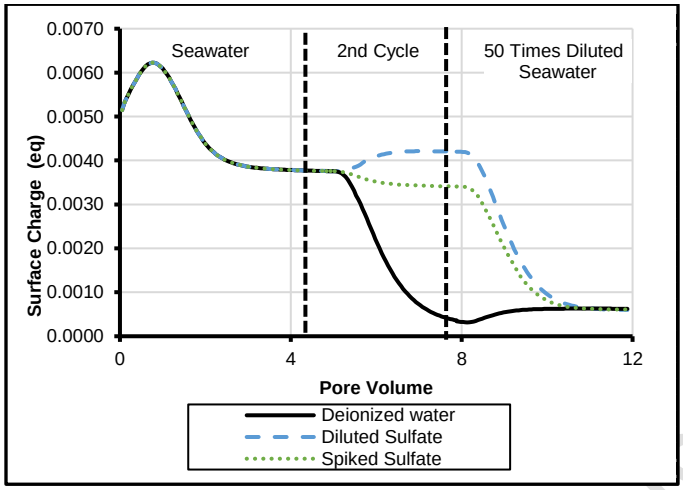

(a)

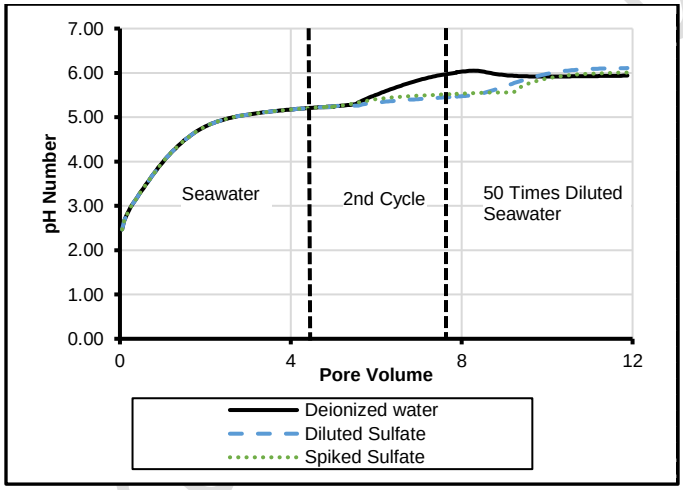

(b)

Fig. 7: Effect of different waters (Deionized, Spiked Sulfate, and Diluted Sulfate) on adsorption at 90 °C and 2nd cycle for (a) Surface charge, (b) pH number.

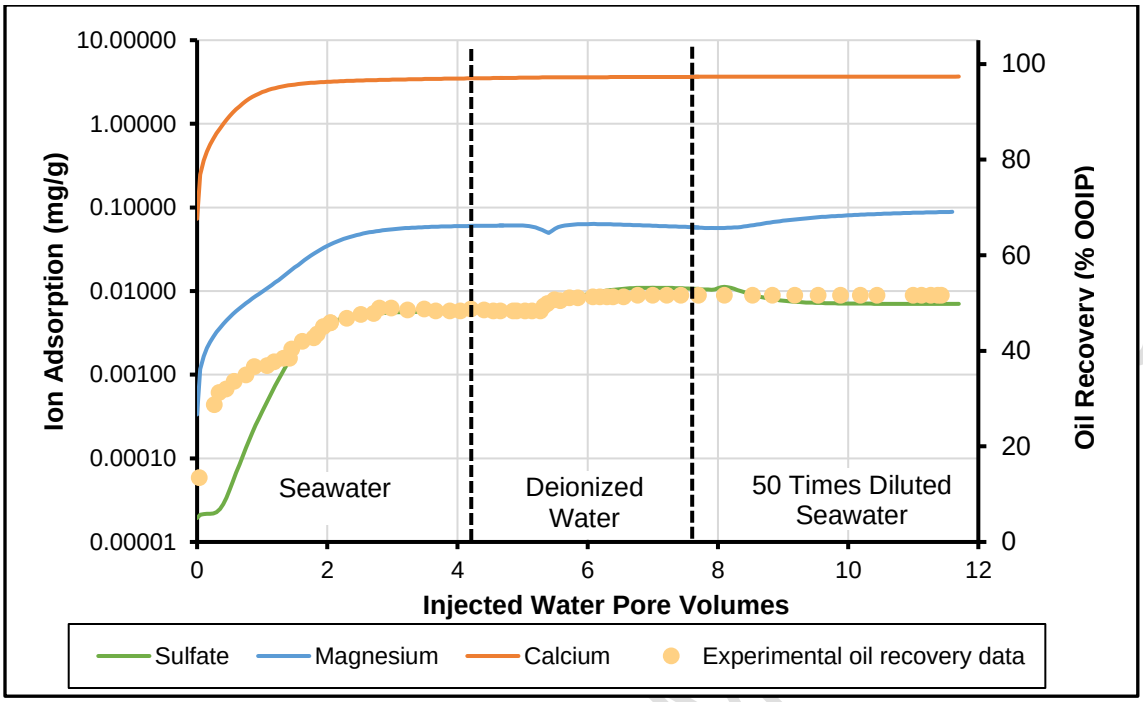

Fig. 8: Oil Recovery data and concentration histories predictions of potential determining ions for the experimental work of Shehata *et al.* [29] at 90 °C.